

Evaluation of the cytotoxic and inflammatory potential of differentially shaped zinc oxide nanoparticles

Boon Chin Heng · Xinxin Zhao · Eng Chok Tan · Nurulain Khamis ·
Aarti Assodani · Sijing Xiong · Christiane Ruedl · Kee Woei Ng ·
Joachim Say-Chye Loo

Received: 21 March 2011 / Accepted: 25 May 2011 / Published online: 9 June 2011
© Springer-Verlag 2011

Abstract Zinc oxide (ZnO) nanoparticles have wide-ranging applications in a diverse array of industrial and consumer products, from ceramic manufacture and paint formulation to sunscreens and haircare products. Hence, it is imperative to rigorously characterize the health and safety aspects of human exposure to ZnO nanoparticles. This study therefore evaluated the cellular association, cytotoxic and inflammatory potential of spherical and sheet-shaped ZnO nanoparticles (of approximately the same specific surface area $\approx 30 \text{ cm}^2/\text{g}$) on mouse and human cell lines (RAW-264.7 and BEAS-2B respectively), as well as with primary cultures of mouse bone marrow-derived dendritic cells (DC). The WST-8 assay demonstrated dose-dependent effects on the cytotoxicity of spherical and sheet-shaped ZnO nanoparticles on both

RAW-264.7 and BEAS-2B cells, even though there was no significant effect of shape on the cytotoxicity of ZnO nanoparticles. There was however higher cellular association of spherical versus sheet-shaped ZnO nanoparticles. Measurement of reactive oxygen species (ROS) with the 2',7'-dichlorofluorescein-diacetate (DCFH-DA) assay indicated up to 4-folds increase in ROS level upon exposure to ZnO nanoparticles, but there was again no significant difference between both ZnO nanoparticle shapes. Exposure of primary dendritic cells to ZnO nanoparticles upregulated expression of CD80 and CD86 (well-known markers of DC activation and maturation) and stimulated release of pro-inflammatory cytokines—IL-6 and TNF- α , thus pointing to the potential of ZnO nanoparticles in inducing inflammation. Hence, our study indicated that ZnO nanoparticles can have potential detrimental effects on cells even at dosages where there are little or no observable cytotoxic effects.

B. C. Heng · X. Zhao · S. Xiong · K. W. Ng · J. S.-C. Loo
School of Materials Science and Engineering, Nanyang Technological University, 60 Nanyang Drive,
Singapore 637551, Singapore

E. C. Tan · N. Khamis · A. Assodani · C. Ruedl
School of Biological Sciences, Nanyang Technological University, Block N4.1, 50 Nanyang Avenue,
Singapore 639798, Singapore

K. W. Ng (✉)
Division of Materials Technology, School of Materials Science and Engineering, Nanyang Technological University, Block N4.1, #02-18, 50 Nanyang Avenue, Singapore 639798, Singapore
e-mail: KWNG@ntu.edu.sg

J. S.-C. Loo (✉)
Division of Materials Technology, School of Materials Science and Engineering, Nanyang Technological University, Block N4.1, #01-04a, 50 Nanyang Avenue, Singapore 639798, Singapore
e-mail: JoachimLoo@ntu.edu.sg

Keywords Cytotoxicity · Inflammation · Nanoparticle · Oxide · Zinc

Introduction

Rapid advances in the field of nanotechnology have created a whole array of nano-sized particles with very different chemical and physical properties as compared to particles in their bulk matter form (Edelstein and Cammarata 1998). Zinc oxide (ZnO) nanoparticles are among the most commonly utilized of nanomaterials, with wide-ranging applications in a diverse arrays of industrial and consumer products, from ceramic manufacture and paint formulation to sunscreens and haircare products (Osmond and McCall 2010; Zvyagin et al. 2008). More recently, ZnO nanoparticles have even been shown to specifically target cancer

cells and can possibly be developed as an alternative anti-cancer therapeutic agent (Hanley et al. 2008). Hence, it is imperative to rigorously characterize the health and safety aspects of human exposure to ZnO nanoparticles.

Although several studies have already characterized the toxicology of ZnO nanoparticles in vitro with a variety of mammalian cell lines (Heng et al. 2010a; Heng et al. 2011; Xia et al. 2008; Yuan et al. 2010), most of these studies focused on the cytotoxicity of ZnO nanoparticles as a means of assessing biocompatibility. Nevertheless, these cytotoxicity assays may not be comprehensive enough for rigorous evaluation of the biocompatibility of nanoparticulate ZnO and more tests characterizing cellular association and inflammation need be carried out to determine the longer-term effects of ZnO nanoparticles on cells. There is much evidence linking inflammation to cancer formation in the long-term (Cole 2009; Hu et al. 2010; Kaluz and Van Meir 2011; O'Callaghan et al. 2010). Hence, it will be prudent to investigate whether ZnO nanoparticles can also induce inflammation besides causing cell death. Another aspect that has been largely overlooked in previous studies on nanoparticulate ZnO is whether altering the shape/size of the nanoparticles can cause variation in their toxicological properties. This study will therefore examine two different shapes of ZnO nanoparticles (spherical and sheet-shaped) with approximately the same specific surface area ($\approx 30 \text{ cm}^2/\text{g}$, Table 1). Spherical ZnO nanoparticles were purchased from a commercially available source (Meliorum Technologies Inc., Rochester, NY, USA), whereas sheet-shaped ZnO nanoparticles were synthesized in house.

The cytotoxicity of the differentially shaped ZnO nanoparticles (spherical and sheet-shaped) was compared using a mouse and human cell line (RAW-264.7 and BEAS-2B, respectively) with the WST-8 assay based on metabolism of a water-soluble tetrazolium salt (Ishiyama et al. 1997). Flow cytometry was utilized to compare cellular association of the differentially shaped ZnO nanoparticles. Subsequently, measurement of reactive oxygen species (ROS) with the 2',7'-dichlorofluorescein-diacetate (DCFH-DA) assay was carried out to determine whether ROS generation could be a possible mechanism in the observed cytotoxicity of ZnO nanoparticles.

The choice of a human bronchial epithelial cell line (BEAS-2B) for this study is based on the fact that the

human respiratory system is often the first line of contact with nanoparticulate environmental pollutants (Schimmer et al. 1997; Zhao et al. 2011). The potential of differentially shaped ZnO nanoparticles to induce inflammatory response will be evaluated by ELISA (enzyme-linked immunosorbent assay) measurement of the secreted levels of tumor necrosis factor alpha (TNF- α) from murine macrophages (RAW-264.7), upon exposure to increasing dosages of ZnO nanoparticles. Macrophages are an important component of the immune system and some of their roles include the detection of foreign bodies, such as bacteria cells and nanoparticles, as well as mediation of inflammation (Raynal et al. 2004). Hence, it is appropriate to study ZnO nanoparticle interaction with a macrophage cell line (RAW-264.7). TNF- α is a pro-inflammatory cytokine that is secreted mainly by macrophages. It is known to trigger the NF- κ B pathway and the MAPK pathway that promotes the anti-apoptotic and pro-apoptotic pathway, respectively (Wajant et al. 2003). Even though TNF- α has been identified as an anti-tumor protein, it has also been linked to cancer induction and progression (Balkwill 2006; Oguma et al. 2010; Sethi et al. 2008; Szlosarek and Balkwill 2003; Williams 2008).

Finally, we also assayed the effects of ZnO nanoparticles on the maturation and cytokine secretion profile of primary cultures of mouse bone marrow-derived dendritic cells (DC), as a means of evaluating their inflammatory potential. Flow cytometry was utilized to determine whether exposure to ZnO nanoparticles can upregulate surface expression levels of two costimulatory molecules—CD80 and CD86, both of which are well-known markers of DC activation and maturation. ELISA was used to determine whether ZnO treatment can stimulate DC to release pro-inflammatory cytokines—IL-6 and TNF- α .

Materials and methods

Cell lines, culture media, reagents, chemicals, and laboratory ware consumables

The human bronchial epithelial cell line (BEAS-2B) and murine macrophage cell line (RAW-264.7) were purchased from the American Type Culture Collection (ATCC,

Table 1 Physical characterization of ZnO nanoparticles

	Hydrodynamic size (nm)	SEM size (nm)	Zeta potential (mV)	Specific surface area (cm^2/g)
Zinc oxide sphere	113	20 × 20	-36 ± 0.2	35.3
Zinc oxide sheet	420	325 × 15	-31 ± 0.3	28.6

Hydrodynamic size and zeta potential of ZnO nanoparticles are measured in SHMP medium. SEM size is determined by measuring the size of 10 random nanoparticles from the SEM picture and then calculating the mean

Manassas, VA, USA). Unless otherwise stated, all reagents and chemicals were purchased from Sigma–Aldrich Inc. (St. Louis, MO, USA), and all culture media, serum, and phosphate buffered saline (PBS) were purchased from PAA Laboratories Inc. (Dartmouth, MA, USA), while all laboratory ware consumables were purchased from Corning Inc. (Corning, NY, USA).

Zinc oxide nanoparticles

Spherical zinc oxide nanoparticles (ZnO sphere) were obtained commercially from Meliorium Technologies Inc. (Rochester, NY, USA). Sheet-shaped zinc oxide nanoparticles (ZnO sheet) were prepared according to a slightly modified method of Usui (2009). Briefly, 6 g of zinc nitrite and 0.32 g of cetyltrimethylammonium bromide (CTAB) were added to 100 ml of distilled water with constant stirring. Subsequently, 1.62 g of sodium hydroxide was added to the solution drop-wise, and the solution was stirred for 1 h, prior to being heated up to 90°C for 4 h within a silica oil bath. After heating, the suspension was cooled gradually to room temperature and the ZnO nanoparticles were then separated from the suspension by centrifugation and washing with ethanol (5 times) and distilled water (5 times), followed by freeze-drying.

Particle characterization

Electron microscopy images were captured with a scanning electron microscope (SEM) (JSM6340-F, JEOL, Tokyo, Japan) at 5 kV and a transmission electron microscope (TEM) (2010 TEM[®]; JEOL, Tokyo, Japan) at an accelerating voltage of 200 kV with a LaB6 cathode. For TEM, samples were prepared by mixing a small quantity of nanoparticles in ethanol, followed by 10 min of ultrasonic treatment and were subsequently collected on carbon-coated copper grids. Particle sizes were measured from the TEM micrographs using the SPOT Basic software (Diagnostic Instruments Inc., Sterling Heights, MI, USA). The hydrodynamic size and zeta potential of the particles were further characterized with dynamic light scattering (Malvern Co., UK) in culture media supplemented with 5% (v/v) fetal bovine serum (FBS) and 0.1% (w/v) sodium hexametaphosphate (SHMP) solution. All samples were sonicated to form colloids prior to testing. Each sample was tested in triplicates and the mean values reported. Hydrodynamic size denotes the size of the nanoparticles within colloidal suspension in aqueous solution. Zeta potential measures the potential difference between the dispersion medium and the layer of fluid around the dispersed nanoparticles within colloidal suspension. It is essentially a measure of the stability of the colloidal

suspension. A zeta potential of between ± 30 and ± 40 mV can be considered stable, while any value below that is considered unstable and aggregation of particles is highly likely. Specific surface area of nanoparticles were analyzed by the Braunauer–Emmet–Teller method (Gelb and Gubbins 1998) with Micromeritics ASAP 2020 (Accelerated Surface Area and Porosimetry Analyzer; Micromeritics Instrument Corp., Norcross, GA, USA). Degassing of nanoparticles was conducted at 120°C for 5 h, prior to analysis.

FITC-labeling of ZnO nanoparticles

Sheet-shaped ZnO nanoparticles were reacted with 3-aminopropyltriethoxysilane (APTES) through a condensation reaction. Briefly, 0.1 g of ZnO nanoparticles and 5 mL APTES in 100 mL of anhydrous ethanol were mixed and refluxed under nitrogen for 3 h with continuous stirring. Subsequently, 0.05 g of FITC was added to the mixture, and the reaction was left overnight at 74°C. The FITC-labeled ZnO was then collected by centrifugation and washed several times with anhydrous ethanol and deionized water to ensure that no free FITC remained, prior to freeze-drying.

Cell culture

Murine peritoneal macrophage cell line RAW-264.7 and human bronchial epithelial cell line BEAS-2B were maintained in Dulbecco's minimum essential medium (DMEM) supplemented with 5% (v/v) FBS (Fetal bovine serum), 2 μ M glutamine and 2 μ M antibiotic/antimycotic solution. When the cells had reached 90% confluence, they were trypsinized with 0.05% (w/v) trypsin (Gibco BRL Inc., Long Island, NY, USA) and subject to serial passage. Primary dendritic cells (DC) were induced from bone marrow progenitors explanted from C57BL/6/J strain mice (Please see later sub-section of “[Materials and methods](#)”).

Cytotoxicity assessment with the WST-8 assay

RAW-264.7 and BEAS-2B cells were plated into 24-well plates at a density of 1.0×10^5 cells per well in 300 μ l of culture media (DMEM supplemented with 5% (w/v) FBS) and incubated for 24 h. Subsequently, the cells were exposed to colloidal suspensions of ZnO sphere and ZnO sheet (with and without FITC-labeling) in culture media (supplemented with 0.1% (w/v) SHMP) at varying concentrations (5 μ g/ml, 10 μ g/ml, 15 μ g/ml, and 20 μ g/ml) for 24 h. Colloidal suspensions of ZnO nanoparticles at various concentrations were sonicated for 15 min prior to incubation with cells. After 24 h, the cells were washed

three times in PBS and incubated for 2 h in 300 μ l of a 9:1 mixture of culture media with WST-8 reagent (Dojindo laboratories Inc., Kumamoto, Japan) to assess cellular metabolic activity (Ishiyama et al. 1997). WST-8 will be reduced by dehydrogenases within cells to produce a yellow-colored formazan product, which is soluble in culture medium (Ishiyama et al. 1997). The amount of the formazan dye generated by the activity of dehydrogenases within cells is therefore directly proportional to the number of living cells. The absorbance of formazan was measured with a microtiter plate reader (Infinite M2000; Tecan Inc., Mannedorf, Switzerland) at a wavelength of 450 nm (reference wavelength 600 nm). Metabolic activity of the ZnO-treated cells was expressed as a percentage of the untreated reference control. Cytotoxicity of ZnO nanoparticles can therefore be assessed and compared by quantifying the reduction in cellular metabolic activity upon nanoparticle exposure.

Cellular association of nanoparticles analyzed with flow cytometry

Cellular association study of ZnO nanoparticles was analyzed with the FACSCalibur Flow Cytometer (Becton–Dickinson Inc., Franklin Lakes, NJ, USA), using FlowJo 7.6 software (Tree Star Inc., Ashland, OR, USA). Cells were seeded into 12-well plates at a density of 5.0×10^5 cells/well for RAW-264.7 cells and 2.0×10^5 cells/well for BEAS-2B cells. After 24 h, the cells were exposed to 15 μ g/ml of either FITC-labeled ZnO sphere or ZnO sheet constituted in culture medium and incubated for 1, 4, and 24 h within the 5% CO₂ incubator. Subsequently, the nanoparticle-treated cells were extensively washed in PBS and detached by trypsinization, followed by fixation in 4% (v/v) paraformaldehyde for 15 min at room temperature. The fixed cells were then pelleted by centrifugation, resuspended in PBS, and stored at 4°C (protected from light), prior to flow cytometry analysis.

DCFH-DA assay for quantification of ROS generation within BEAS-2B cells exposed to zinc oxide nanoparticles

Intracellular ROS levels within ZnO-treated cells were measured with the 2',7'-dichlorofluorescein-diacetate (DCFH-DA) assay, using a modified method of Qin et al. (2005). DCFH-DA enters the cells passively and forms fluorescent dihydrofluorescein (DHF) upon reaction with ROS within the cells. A working solution of 10 μ M of DCFH-DA (Sigma–Aldrich Inc, St. Louis, MO, USA) in PBS was prepared. BEAS-2B cells were seeded at a density of 5.0×10^4 cells per well within a 96-well opaque plate and incubated for 24 h in a 5% CO₂ humidified

environment. The cells were then exposed to spherical and sheet-shaped ZnO nanoparticles at varying concentrations (2.5, 5, 10, and 20 μ g/ml) and incubated for 24 h, prior to being washed three times with PBS and incubated with 2 ml of 10 μ M DCFH-DA working solution at 37°C for 30 min. Subsequently, the cells were washed again three times in PBS to remove excess DCFH-DA, and the DHF fluorescence intensity was measured at excitation/emission wavelengths of 488 nm/525 nm emission with a microplate reader (Infinite M2000; Tecan Inc., Mannedorf, Switzerland).

ELISA measurement of TNF- α secretion by cells exposed to zinc oxide nanoparticles

RAW 264.7 cells were seeded at a density of 5.0×10^4 cells per well of a 96 well-plate and incubated for 24 h, prior to being exposed to varying concentrations (0.3, 1, 3, and 10 μ g/ml) of spherical and sheet-shaped ZnO nanoparticles. Fifty microliter supernatants were collected at a time-point of 6 h and mixed with 50 μ l of DMEM, prior to being stored at 4°C. TNF- α level within the supernatants was quantified with a mouse TNF- α ELISA kit (Biolegend Inc., San Diego, CA, USA) following the manufacturer's instruction with slight modification. Briefly, mouse TNF- α capture antibody was diluted 200 times in PBS solution, and 100 μ l of the diluted TNF- α capture antibody was added to each well and incubated at 4°C for 24 h. The plates were then washed with PBS containing 1% (v/v) Tween-20 solution (PBS-T) to remove any unbound capture antibody. To block non-specific binding, 100 μ l of PBS containing 0.5% (w/v) bovine serum albumin (PBS-BSA) was added to each well and incubated for 2 h. Subsequently, the plates were washed with PBS-T four times before loading 100 μ l of the samples into each well and incubating for 2 h. The TNF- α standard was diluted to 500 pg/ml, and a log 2 serial dilution was carried out prior to loading onto the plate. Blank PBS and DMEM control were also added to the plate and incubated for 2 h. After incubation, the plates were washed with PBS-T four times. The detection antibody was diluted 200 times in PBS-T solution, and 100 μ l of the diluted solution was added to each well and incubated for 2 h. The plates were washed again with PBS-T four times before the addition of avidin-HRP (horse radish peroxidase). After 30 min incubation, the plates were washed four times with PBS-T. TMB substrate A and B were then mixed in a 1:1 ratio, and 100 μ l of the mixture was added to each well. Finally after 5 min, the absorbance was measured at 370 nm using a plate reader (Multiskan Spectrum, ThermoScientific Inc., Waltham, MA, USA). A standard curve was plotted, from which the quantity of TNF- α in the test samples were determined.

Harvesting of bone marrow progenitors and subsequent induction to dendritic cells (DC)

Femurs and tibias were isolated from C57BL/6/J mouse cadavers, and cells were flushed out using PBS supplemented with 2% (v/v) FCS (fetal calf serum) through a 26G 1/2 needle (BD). Contaminating Erythrocytes were lysed by exposure to 0.89% (w/v) ammonium chloride for 10 min at room temperature. The remaining cells were then re-suspended in 20 mL of culture media comprised of Iscove's Modified Dulbecco's Medium (IMDM) supplemented with 2% (w/v) FCS, 100 µg/ml Ciprofloxacin (antibiotic), and 100 ng/ml of the cytokine Flt-3L (Santa Cruz Biotechnology Inc., Santa Cruz, CA, USA). Subsequently, the cell suspension was filtered through a metal sieve prior to seeding into 60 × 15 mm cell culture dishes at a density of 1.5×10^7 cells/plate. The cells were cultured for 7 days within an incubator set at 37°C incubator and 7% CO₂. Fresh culture medium containing Flt-3L was replaced on day 4. Flt3-L generated dendritic cells (DCs)

were then magnetically sorted to enrich the CD11b+ population as per manufacturer's instructions (CD11b+ Microbeads; Miltenyi Biotec GmbH, Bergisch Gladbach, Germany).

Effects of ZnO nanoparticles on bone marrow-derived dendritic cell (DC) maturation and secretion of inflammatory cytokines

ZnO nanoparticles were tested for their capacity to modulate maturation of dendritic cells. Flt3L-derived bone marrow CD11b⁺ DCs were co-cultured for 24 h with a range of 1–30 µg/ml spherical and sheet-shaped ZnO nanoparticles and were subsequently analyzed for the surface expression levels of two costimulatory molecules—CD80 and CD86, both of which are well-known markers of DC activation and maturation. Antibodies specific for CD80, CD86 (Biolegend Inc., San Diego, CA, USA) were used to monitor the maturation state of DCs. Mean of fluorescence intensity was assessed by flow cytometry

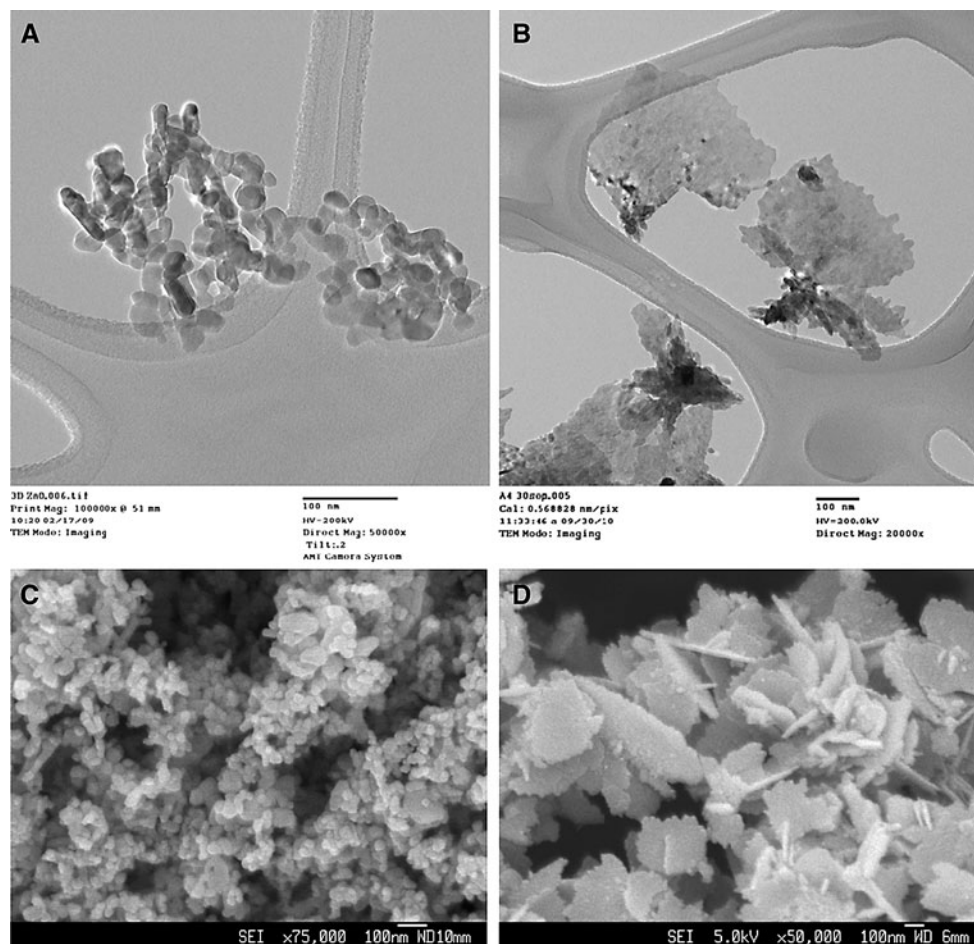


Fig. 1 Transmission electron microscope (TEM) images of **a** ZnO sphere and **b** ZnO sheet; and scanning electron microscope images of **c** ZnO sphere and **d** ZnO sheet

(FACScalibur®, Becton Dickinson, Franklin Lakes, NJ, USA). IL-6 and TNF- α release was measured in the culture supernatants by ELISA (Biolegend Inc., San Diego, CA, USA).

Calculation and statistical analysis

Statistical analysis was carried out with GraphPad Prism 5 statistical software (Graphpad Software Inc., La Jolla, CA, USA). Values are presented as mean \pm standard deviation (STD) of 3 independent replicate experiments, unless stated otherwise. Statistical comparisons between treatment groups were performed with 1-way ANOVA, followed by a Dunnett's Multiple Comparison Test. Differences were considered statistically significant when the P value was less than 0.05.

Results

Particle characterization

Spherical and sheet-shaped ZnO nanoparticles were characterized through a variety of parameters, including hydrodynamic size, zeta potential, SEM, and TEM (Fig. 1). Table 1 summarizes the characterization of ZnO nanoparticles of both shapes.

Cytotoxicity assessment with the WST-8 assay

After 24 h exposure to varying doses of spherical and sheet-shaped ZnO nanoparticles, cellular metabolic activity detected by the WST-8 assay indicated a dose-dependent effect on cytotoxicity for both RAW-264.7 and BEAS-2B cells (Fig. 2a, b), with the extrapolated LD₅₀ values of ZnO sphere and ZnO sheet being presented in Table 2. The LD₅₀ values indicated that ZnO sphere is slightly more toxic than ZnO sheet for both cell lines however differences were not significantly different ($P > 0.05$). Additionally, it was observed that differentially shaped ZnO nanoparticles displayed variation in their cytotoxic effects on the 2 cell lines ($P < 0.05$) (Fig. 3), with RAW-264.7 cells appearing to be more sensitive to ZnO sphere compared with BEASB-2B cells, particularly at higher concentrations of 15 and 20 $\mu\text{g/ml}$ (Fig. 3a). Differences were significant at 15 $\mu\text{g/ml}$ ($P < 0.05$), but not at 20 $\mu\text{g/ml}$ ($P > 0.05$). FITC-labeling did not significantly alter the cytotoxicity of sheet-shaped ZnO nanoparticles on both cell lines at lower concentrations of 5, 10, and 15 $\mu\text{g/ml}$ (Fig. 4). However, at 20 $\mu\text{g/ml}$, FITC-labeling caused a significant reduction in the cytotoxicity of ZnO sheet ($P < 0.05$, Fig. 4).

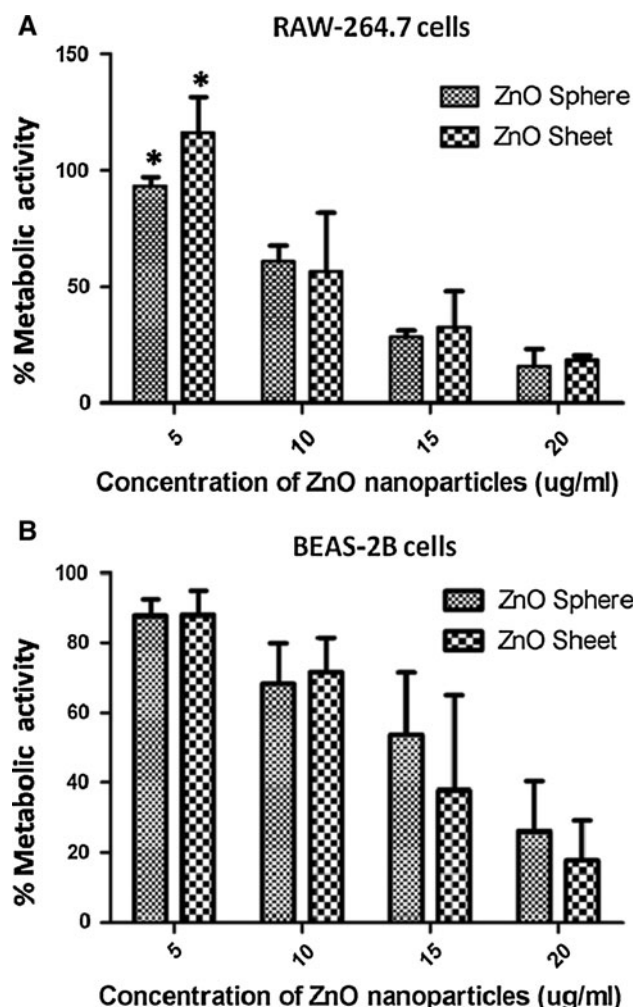


Fig. 2 Percentage metabolic activity of **a** RAW-264.7 and **b** BEAS-2B cells upon exposure to varying concentrations of ZnO nanoparticles, as determined by the WST-assay. Cells were treated with 5, 10, 15, and 20 $\mu\text{g/ml}$ of spherical and sheet-shaped ZnO nanoparticles for 24 h. The results are expressed as a percentage relative to controls and are presented as mean \pm SD of three independent replicate experiments. * denotes statistically significant difference ($P < 0.05$)

Table 2 Extrapolated LD₅₀ values of zinc oxide nanoparticles

	LD ₅₀ ($\mu\text{g/ml}$) for RAW 264.7	LD ₅₀ ($\mu\text{g/ml}$) for BEAS2B
Zinc oxide sphere	11.7	13.3
Zinc oxide sheet	12.3	16.0

Cellular association of ZnO nanoparticles analyzed with flow cytometry

The flow cytometry results are presented as dot plots—forward scatter against fluorescence intensity—as shown in

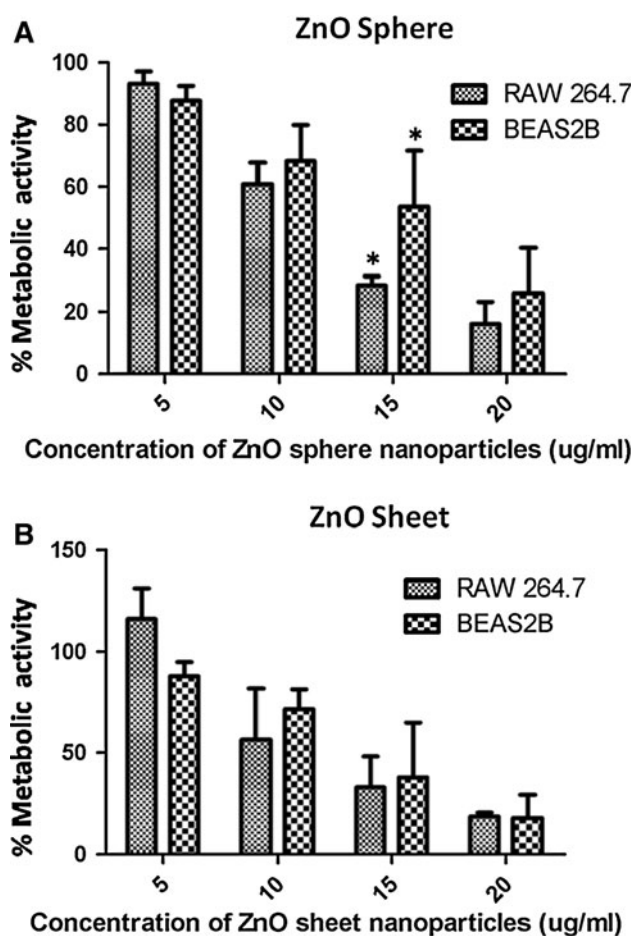


Fig. 3 Comparison of metabolic activity of RAW-264.7 and BEAS-2B cells upon exposure to **a** spherical and **b** sheet-shaped ZnO nanoparticles. * denotes statistically significant difference ($P < 0.05$)

Fig. 5. Statistics showing the percentage of cells that have taken up the FITC-labeled ZnO nanoparticles are also summarized in Fig. 5. The results showed that the percentage of BEAS-2B cells that have taken up the FITC-labeled ZnO nanoparticles was highest at 4 h and then decreased at the 24 h time-point (Fig. 5). Upon comparing the association of ZnO sphere and ZnO sheet with BEAS-2B cells, the flow cytometry data showed conclusively that more ZnO sphere nanoparticles were taken up as compared to ZnO sheet nanoparticles at all 3 time points. Data on the cellular association of ZnO nanoparticles with RAW-264.7 cells were not presented in this study as the results were inconclusive due to difficulty in detaching and dissociating the nanoparticle-treated RAW-264.7 cells, even after extensive washing and trypsinization. Our preliminary observation is that exposure to ZnO nanoparticles somehow made it difficult to detach and dissociate RAW-264.7 cells with trypsin. This observed phenomenon may be worthwhile investigating in future studies. To overcome

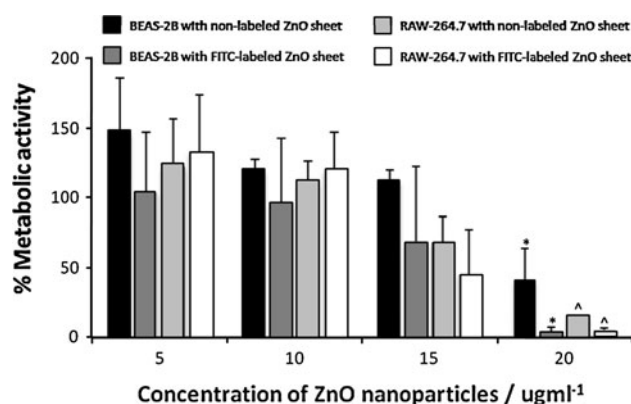


Fig. 4 Comparison of the effects of non-labeled versus FITC-labeled ZnO sheet nanoparticles on the metabolic activity of BEAS-2B cells. Cells were treated with 5, 10, 15, and 20 $\mu\text{g/ml}$ of non-labeled and FITC-labeled ZnO sheet for 24 h. The results are given in percentage relative to controls. Data were presented as mean \pm SD of 2 independent experiments with at least 3 replicates. *, ^ denote statistically significant differences ($P < 0.05$)

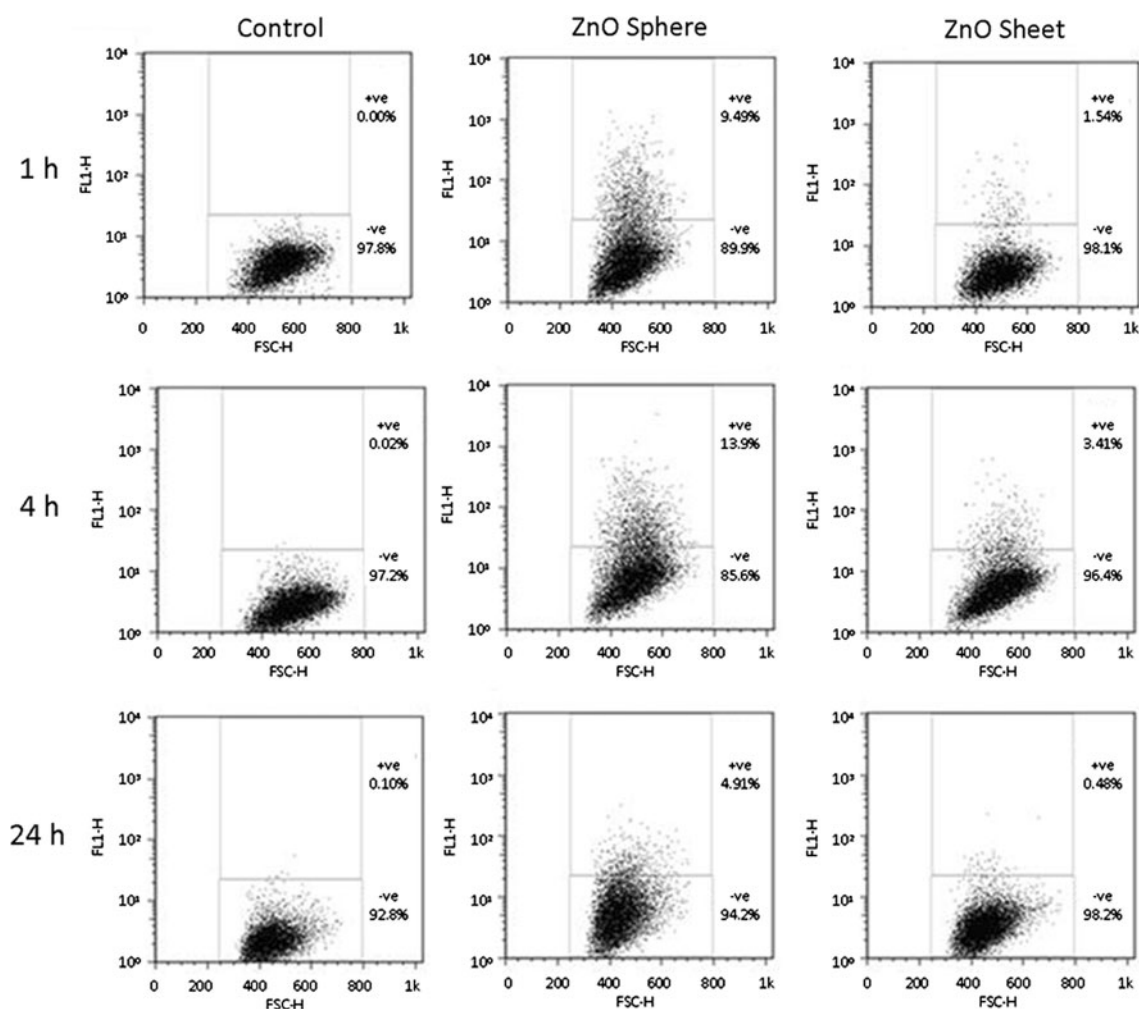
this problem, we attempted to scrape off the cells from the plate before transferring to a centrifuge tube. However, scraping of the cells could rupture the cell membrane and lead to cell death that may in turn skew the experimental data. Moreover, flow cytometry analysis requires thorough dissociation of the monolayer into a single-cell suspension, whereas we obtained multi-cellular clumps with the nanoparticle-treated RAW-264.7 cells, even after extensive trypsinization and vigorous pipeting.

DCFH-DA assay for quantification of ROS generation within BEAS-2B cells exposed to zinc oxide nanoparticles

ROS production level in BEAS-2B cells exhibited a dose-dependent increase after 4 h exposure to spherical and sheet-shaped ZnO nanoparticles (Fig. 6). ZnO sphere appears to induce more ROS production than ZnO sheet, particularly at higher concentrations of 10 and 20 $\mu\text{g/ml}$. Differences were significant ($P < 0.05$) at 20 $\mu\text{g/ml}$, but not at 10 $\mu\text{g/ml}$. This may be attributed to the difference in cytotoxicity of ZnO sheet versus ZnO sphere.

ELISA measurement of TNF- α secretion by cells exposed to zinc oxide nanoparticles

RAW 264.7 cells exhibited a dose-dependent increase in TNF- α production after 6 h exposure to ZnO nanoparticles (Fig. 7). Both spherical and sheet-shaped ZnO nanoparticles at a low concentration of 0.3 $\mu\text{g/ml}$ induced as much as 200-fold increase in TNF- α production compared with the untreated control. Additionally, it was observed that ZnO sphere significantly induced more TNF- α production compared with ZnO sheet ($P < 0.05$).



ZnO nanoparticle shape	Incubation time (h)	*Percentage Gated (%)
Sphere	1	9.5
	4	13.9
	24	4.9
Sheet	1	1.5
	4	3.4
	24	0.5

*Percentage gated refers to the percentage of cells that took up the nanoparticles.

Fig. 5 Flow cytometry analysis of the cellular association of ZnO nanoparticles with BEAS-2B cells at different time points. Dot plot—forward scatter against fluorescence intensity—was used to represent

the results. Positive section (+ve) referred to cells that have taken up the nanoparticles

Zinc oxide nanoparticles induce dendritic cell maturation and priming of inflammatory cytokine release

As shown in Fig. 8a, the highest tested concentration of both spherical and sheet-shaped ZnO nanoparticles clearly

upregulated CD80 and CD86 expression, thus, pointing to an induction/activation of the treated dendritic cells. Subsequently, we analyzed whether the ZnO nanoparticles also stimulated the secretion of pro-inflammatory cytokines, another hall-mark of the DC activation process. IL-6 and TNF- α secretion levels were observed to be significantly

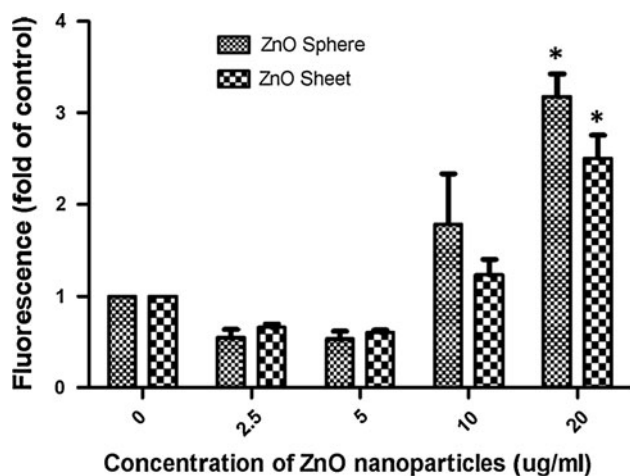


Fig. 6 Effects of ZnO nanoparticle-induced ROS generation in BEAS-2B cells, as determined by DCFH-DA assay. Cells were treated with 2.5, 5, 10, and 20 $\mu\text{g/ml}$ of ZnO nanoparticles and incubated for 4 h. Results are presented as mean \pm SD of 2 independent replicate experiments. * denotes statistically significant difference ($P < 0.05$)

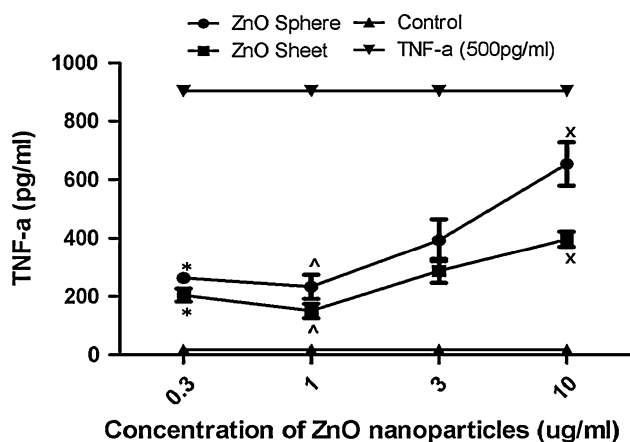


Fig. 7 TNF- α level in RAW-264.7 cells exposed to ZnO nanoparticles for 6 h as determined by ELISA. A positive (TNF- α) and blank control (DMEM) are included as comparison. Results are presented as mean \pm SD of three independent replicate experiments. *, ^, ^x denote statistically significant differences ($P < 0.05$)

increased upon exposure to ZnO nanoparticles of both shapes, with the ZnO sheet exerting a greater stimulatory effect (Fig. 8b).

Discussion

Previous studies have reported that the size and shape of ZnO nanoparticles could profoundly influence their cytotoxic effects (Hsiao and Huang 2011; Nair et al. 2009), aggregation kinetics in solution (Zhou and Keller 2010), and catalytic properties (Raula et al. 2010). This study therefore sought to investigate whether spherical and sheet-

shaped ZnO nanoparticles of the same specific surface area ($30 \text{ cm}^2/\text{g}$) could display differences in their cytotoxic and inflammatory potential. Spherical-shaped ZnO nanoparticles are commonly utilized for various industrial applications, whereas sheet-shaped ZnO nanoparticles could have potential applications in solar cell technology (Xiang et al. 2006). Recently, Xiang et al. (2006) demonstrated that the ZnO nanosheet microstructure was able to reduce loss during photoelectron transport, increase dye compound adsorption, and enhance the incidence of light capture in solar cells.

Even though nanoparticles can be synthesized easily, it is difficult to maintain their nano-size in the actual real-life situation. Due to their high specific surface area and high surface energy level, nanoparticles have the propensity to aggregate together to form micro-size particles that are more stable in the environment (He et al. 2006; Petosa et al. 2010). This effect is more evident when nanoparticles are suspended in cell culture medium. The particles will tend to aggregate and sediment to the bottom of the well after some time. Hence, the observed discrepancy in particle size, as measured by dynamic light scattering and electron microscopy (Table 1). To minimize the effects of particles aggregation and sedimentation, colloidal suspension of ZnO nanoparticles were always freshly prepared and sonicated before each experiment.

In this study, the cytotoxicity of differentially shaped ZnO nanoparticles were assessed and compared with the WST-8 assay based on cellular metabolic activity. Previous studies by our group have demonstrated that the presentation of WST-8 assay data in terms of cell viability may be flawed due to the differential effects of nanoparticles on cellular metabolism (Heng et al. 2010b; Ng et al. 2005). Hence, the WST-8 assay data in this study were more appropriately presented in terms of metabolic activity instead of cell viability (Figs. 2, 3 and 4). The lack of statistically significant differences in the WST-8 assay data (Table 2, Fig. 2a, b) may suggest that the morphology of ZnO nanoparticles does not affect cytotoxicity to a large extent. Previous studies have suggested that toxicity of ZnO nanoparticles are a result of dissolution and subsequent release of Zn^{2+} ions that are toxic to cells (Xia et al. 2008). The observed slight difference in cytotoxicity of spherical versus sheet-shaped ZnO nanoparticles may be due to differences in the dissolution rate that occur as a result of differences in size and shape (Meulenkamp 1998). The observed slight increase in the metabolic activity of RAW-264.7 cells upon treatment with 5 $\mu\text{g/ml}$ of ZnO sheet particles (Fig. 2a) may be due to increase metabolism of RAW-264.7 cells as they phagocytosed the nanoparticles. The lack of a similar trend for BEAS-2B cells that have less propensity to phagocytose ZnO nanoparticles

Fig. 8 Effects of ZnO nanoparticles on expression of a CD80 and CD86 (FACS analysis) and b secretion of pro-inflammatory cytokines—IL-6 and TNF- α (ELISA) by mouse primary dendritic cells. *, \wedge , \times denote statistically significant differences ($P < 0.05$)

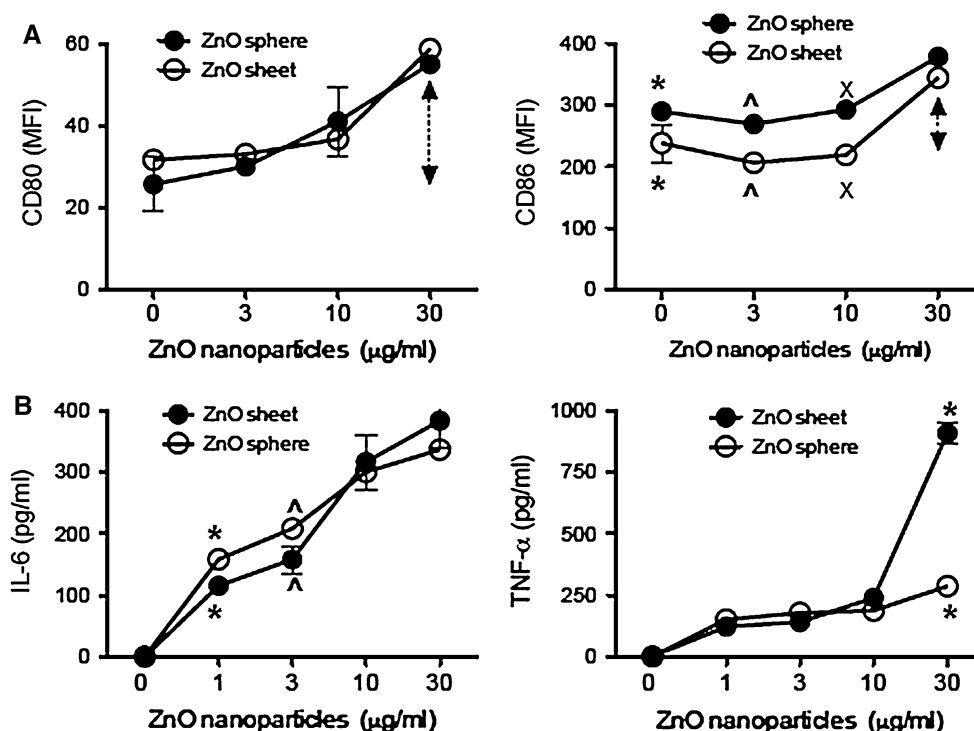


(Fig. 2b) further confirmed our hypothesis. The observation that RAW-264.7 cells are more sensitive to ZnO nanoparticle-induced cytotoxicity compared with BEAS-2B cells could thus indicate that the mechanism of ZnO nanoparticle cytotoxicity may involve phagocytosis. An increase in cellular association of nanoparticles due to phagocytosis may contribute to the observed increased sensitivity of RAW-264.7 cells to ZnO nanoparticles. Another possible explanation may involve ZnO nanoparticles binding to RAW-264.7 cell-specific receptors and triggering apoptotic pathways (Grandjean-Laquerriere et al. 2007).

In this study, we also tried to characterize the association of ZnO nanoparticles with BEAS-2B and RAW-264.7 cells. The observed higher cellular association of ZnO sphere versus ZnO sheet could be due to the smaller size of the ZnO sphere nanoparticles. Additionally, it was observed that the cellular association of ZnO nanoparticles was maximal at the 4 h time-point and declined thereafter. The decrease in the percentage of cells that took up ZnO nanoparticles at the 24 h time-point (Fig. 5) may be due to exocytosis of ZnO nanoparticles after these have been taken up and accumulated within the cell. Our results are consistent with that of a previous study by Kennedy et al. (2009), which showed that iron (III) oxide (Fe_2O_3) can be exocytosed by HAECs cells after 4 h exposure to Fe_2O_3 nanoparticles. No doubt different cells and nanoparticles were utilized in the study of Kennedy et al. (2009), but their result can provide an insight for the cellular

association of ZnO nanoparticles with BEAS-2B cells. As mentioned earlier, data on the cellular association of ZnO nanoparticles with RAW-264.7 cells was not presented in this study as the results were inconclusive due to the difficulty in detaching and dissociating the nanoparticle-treated RAW-264.7 cells, even after extensive washing and trypsinization.

The observed higher degree of cellular association of spherical versus sheet-shaped ZnO nanoparticles could make spherical ZnO nanoparticles more useful for the selective destruction of tumor cells and for drug delivery applications (Wahab et al. 2011). A number of previous studies have reported that ZnO nanoparticles exhibited much higher cytotoxic effects on malignant cancerous cells compared with normal cells (Hackenberg et al. 2010; Hanley et al. 2008; Hsiao and Huang 2011; Nair et al. 2009; Rasmussen et al. 2010; Wahab et al. 2011), which makes them potential therapeutic agents for cancer treatment. Although no significant differences were observed in the cytotoxicity of spherical and sheet-shaped ZnO nanoparticles on BEAS-2B and Raw 264.7 cells in this study, previous studies have reported profound effects of ZnO nanoparticle size and shape on their cytotoxic effects on A549 human lung epithelial cells (Hsiao and Huang 2011) and osteoblast cancer cells (Nair et al. 2009). Probably, the differential effects of size and shape of ZnO nanoparticles on their cytotoxicity are also very much dependent on the specific cell type. This needs to be further investigated in future studies.

Previous studies have linked ROS generation to inflammation (Gill et al. 2010; Khodr and Khalil 2001; Lonkar and Dedon 2011). The observed increase in TNF- α secretion upon exposure to ZnO nanoparticles may again be attributed to ROS production even though other factors such as activation of inflammatory signaling pathways cannot be ruled out. Furthermore, both shapes of ZnO nanoparticles were shown to induce DC maturation and activation. Indeed, upregulation of co-stimulatory molecules (CD80 and CD86), as well as priming of pro-inflammatory cytokine secretion (IL-6 and TNF- α) could be visualized upon the treatment of primary dendritic cells with ZnO nanoparticles (Fig. 8), thus pointing to the potential of this material in inducing inflammation.

The results of this study therefore demonstrated that while there was no significant difference in the cytotoxicity of ZnO sphere versus ZnO sheet, other experimental data indicated that there were differences in the cellular association and inflammatory potential of ZnO nanoparticles of different shapes. These effects were significant even at relatively low concentrations (<5 $\mu\text{g/ml}$) of ZnO nanoparticles, where cellular metabolic activity is high. Hence, evaluation of the biocompatibility of newly formulated nanomaterials should not focus on cytotoxicity alone, but should also encompass longer-term side effects that nanoparticles could potentially inflict on cells, such as inflammation.

References

- Balkwill F (2006) TNF-alpha in promotion and progression of cancer. *Cancer Metastasis Rev* 25(3):409–416
- Cole SW (2009) Chronic inflammation and breast cancer recurrence. *J Clin Oncol* 27(21):3418–3419
- Edelstein AS, Cammarata RC (1998) *Nanomaterials: synthesis, properties and applications*, 2nd edn. Taylor and Francis, London
- Gelb LD, Gubbins KE (1998) Characterization of porous glasses: simulation models, adsorption isotherms, and the Brunauer–Emmett–Teller analysis method. *Langmuir* 14(8):2097–2111
- Gill R, Tsung A, Billiar T (2010) Linking oxidative stress to inflammation: toll-like receptors. *Free Radic Biol Med* 48(9):1121–1132
- Grandjean-Laquerriere A, Tabary O, Jacquot J, Richard D, Frayssinet P, Guenounou M, Laurent-Maquin D, Laquerriere P, Gangloff S (2007) Involvement of toll-like receptor 4 in the inflammatory reaction induced by hydroxyapatite particles. *Biomaterials* 28(3):400–404
- Hackenberg S, Scherzed A, Kessler M, Froelich K, Ginzkey C, Koehler C, Burghartz M, Hagen R, Kleinsasser N (2010) Zinc oxide nanoparticles induce photocatalytic cell death in human head and neck squamous cell carcinoma cell lines in vitro. *Int J Oncol* 37(6):1583–1590
- Hanley C, Layne J, Punnoose A, Reddy KM, Coombs I, Coombs A, Feris K, Wingett D (2008) Preferential killing of cancer cells and activated human T cells using ZnO nanoparticles. *Nanotechnol* 19(29):295103
- He YT, Wan J, Tokunaga T (2006) Kinetic stability of hematite nanoparticles: the effect of particle sizes. *J Nanoparticle Res* 10(2):321–332
- Heng BC, Zhao X, Xiong S, Ng KW, Boey FY, Loo JSC (2010a) Toxicity of zinc oxide (ZnO) nanoparticles on human bronchial epithelial cells (BEAS-2B) is accentuated by oxidative stress. *Food Chem Toxicol* 48(6):1762–1766
- Heng BC, Das GK, Zhao X, Ma LL, Tan TT, Ng KW, Loo JSC (2010b) Comparative cytotoxicity evaluation of lanthanide nanomaterials on mouse and human cell lines with metabolic and DNA-quantification assays. *Biointerphases* 5(3):88–97
- Heng BC, Zhao X, Xiong S, Ng KW, Boey FY, Loo JSC (2011) Cytotoxicity of zinc oxide (ZnO) nanoparticles is influenced by cell density and culture format. *Archives of Toxicology* (in press). doi: 10.1007/s00204-010-0608-7
- Hsiao IL, Huang YJ (2011) Effects of various physicochemical characteristics on the toxicities of ZnO and TiO nanoparticles toward human lung epithelial cells. *Sci Total Environ* 409(7):1219–1228
- Hu B, Elinav E, Huber S, Booth CJ, Strowig T, Jin C, Eisenbarth SC, Flavell RA (2010) Inflammation-induced tumorigenesis in the colon is regulated by caspase-1 and NLR4. *Proc Natl Acad Sci USA* 107(50):21635–21640
- Ishiyama M, Miyazono Y, Sasamoto K, Ohkura Y, Ueno K (1997) A highly water-soluble disulfonated tetrazolium salt as a chromogenic indicator for NADH as well as cell viability. *Talanta* 44(7):1299–1305
- Kaluz S, Van Meir EG (2011) At the crossroads of cancer and inflammation: ras rewires an HIF-driven IL-1 autocrine loop. *J Mol Med* 89(2):91–94
- Kennedy IM, Wilson D, Barakat AI, HEI Health Review Committee (2009) Uptake and inflammatory effects of nanoparticles in a human vascular endothelial cell line. *Res Rep Health Eff Inst* (136):3–32
- Khodr B, Khalil Z (2001) Modulation of inflammation by reactive oxygen species: implications for aging and tissue repair. *Free Radic Biol Med* 30(1):1–8
- Lonkar P, Dedon PC (2011) Reactive species and DNA damage in chronic inflammation: reconciling chemical mechanisms and biological fates. *Int J Cancer* 128(9):1999–2009
- Meulenkamp EA (1998) Size dependence of the dissolution of zno nanoparticles. *J Physical Chem B* 102:7764–7769
- Nair S, Sasidharan A, Divya Rani VV, Menon D, Nair S, Manzoor K, Raina S (2009) Role of size scale of ZnO nanoparticles and microparticles on toxicity toward bacteria and osteoblast cancer cells. *J Mater Sci Mater Med* 20(Suppl 1):235–241
- Ng KW, Leong DT, Hutmacher DW (2005) The challenge to measure cell proliferation in two and three dimensions. *Tissue Eng* 11(1–2):182–191
- O’Callaghan DS, O’Donnell D, O’Connell F, O’Byrne KJ (2010) The role of inflammation in the pathogenesis of non-small cell lung cancer. *J Thorac Oncol* 5(12):2024–2036
- Oguma K, Oshima H, Oshima M (2010) Inflammation, tumor necrosis factor and Wnt promotion in gastric cancer development. *Future Oncol* 6(4):515–526
- Osmond MJ, McCall MJ (2010) Zinc oxide nanoparticles in modern sunscreens: an analysis of potential exposure and hazard. *Nanotoxicology* 4(1):15–41
- Petosa AR, Jaisi DP, Quevedo IR, Elimelech M, Tufenkji N (2010) Aggregation and deposition of engineered nanomaterials in aquatic environments: role of physicochemical interactions. *Environ Sci Technol* 44(17):6532–6549
- Qin L, Block ML, Liu Y, Bienstock RJ, Pei Z, Zhang W, Wu X, Wilson B, Burka T, Hong JS (2005) Microglial NADPH oxidase is a novel target for femtomolar neuroprotection against oxidative stress. *FASEB J* 19(6):550–557

- Rasmussen JW, Martinez E, Louka P, Wingett DG (2010) Zinc oxide nanoparticles for selective destruction of tumor cells and potential for drug delivery applications. *Expert Opin Drug Deliv* 7(9):1063–1077
- Raula M, Rashid MH, Paira TK, Dinda E, Mandal TK (2010) Ascorbate-assisted growth of hierarchical ZnO nanostructures: sphere, spindle, and flower and their catalytic properties. *Langmuir* 26(11):8769–8782
- Raynal I, Prigent P, Peyramaure S, Najid A, Rebutzi C, Corot C (2004) Macrophage endocytosis of superparamagnetic iron oxide nanoparticles: mechanisms and comparison of ferumoxides and ferumoxtran-10. *Invest Radiol* 39(1):56–63
- Schimmer RC, Schrier DJ, Flory CM, Dykens J, Tung DK, Jacobson PB, Friedl HP, Conroy MC, Schimmer BB, Ward PA (1997) Streptococcal cell wall-induced arthritis requirements for neutrophils, P-selectin, intercellular adhesion molecule-1, and macrophage-inflammatory protein-2. *J Immunol* 159(8):4103–4108
- Sethi G, Sung B, Aggarwal BB (2008) TNF: a master switch for inflammation to cancer. *Front Biosci* 13:5094–5107
- Szlosarek PW, Balkwill FR (2003) Tumour necrosis factor alpha: a potential target for the therapy of solid tumours. *Lancet Oncol* 4(9):565–573
- Usui H (2009) Surfactant concentration dependence of structure and photocatalytic properties of zinc oxide rods prepared using chemical synthesis in aqueous solutions. *J Colloid Interface Sci* 336(2):667–674
- Wahab R, Kaushik NK, Verma AK, Mishra A, Hwang IH, Yang YB, Shin HS, Kim YS (2011) Fabrication and growth mechanism of ZnO nanostructures and their cytotoxic effect on human brain tumor U87, cervical cancer HeLa, and normal HEK cells. *J Biol Inorg Chem* 16(3):431–442
- Wajant H, Pfizenmaier K, Scheurich P (2003) Tumor necrosis factor signaling. *Cell Death Differ* 10(1):45–65
- Williams GM (2008) Antitumor necrosis factor-alpha therapy and potential cancer inhibition. *Eur J Cancer Prev* 17(2):169–177
- Xia T, Kovoichich M, Liang M, Mädler L, Gilbert B, Shi H, Yeh JI, Zink JI, Nel AE (2008) Comparison of the mechanism of toxicity of zinc oxide and cerium oxide nanoparticles based on dissolution and oxidative stress properties. *ACS Nano* 2(10):2121–2134
- Xiang JH, Zhu PX, Masuda Y, Okuya M, Kaneko S, Koumoto K (2006) Flexible solar-cell from zinc oxide nanocrystalline sheets self-assembled by an in situ electrodeposition process. *J Nanosci Nanotechnol* 6(6):1797–1801
- Yuan JH, Chen Y, Zha HX, Song LJ, Li CY, Li JQ, Xia XH (2010) Determination, characterization and cytotoxicity on HELF cells of ZnO nanoparticles. *Colloids Surf B Biointerfaces* 76(1):145–150
- Zhao X, Heng BC, Guo J, Tan TT, Ng KW, Loo SC (2011) In vitro assessment of cellular responses to the length effect of rod shaped nano-sized hydroxyapatite. *Nanotoxicology* (in press). doi: [10.3109/17435390.2010.503943](https://doi.org/10.3109/17435390.2010.503943)
- Zhou D, Keller AA (2010) Role of morphology in the aggregation kinetics of ZnO nanoparticles. *Water Res* 44(9):2948–2956
- Zvyagin AV, Zhao X, Gierden A, Sanchez W, Ross JA, Roberts MS (2008) Imaging of zinc oxide nanoparticle penetration in human skin in vitro and in vivo. *J Biomed Opt* 13(6):064031